Immune-responsive gene 1 protein links metabolism to immunity by catalyzing itaconic acid production

Alessandro Michelucci[a,1], Thekla Cordes[a,1], Jenny Ghelfi[a], Arnaud Pailot[a], Norbert Reiling[b], Oliver Goldmann[c], Tina Binz[a], André Wegner[a], Aravind Tallam[a], Antonio Rausell[a], Manuel Buttini[a], Carole L. Linster[a], Eva Medina[c], Rudi Balling[a], and Karsten Hiller[a,2]

[a]Luxembourg Centre for Systems Biomedicine, University of Luxembourg, L-4362 Esch-Belval, Luxembourg; [b]Division of Microbial Interface Biology, Research Center Borstel, Leibniz Center for Medicine and Biosciences, 23845 Borstel, Germany; and [c]Infection Immunology Research Group, Helmholtz Centre for Infection Research, 38124 Braunschweig, Germany

Edited by Philippa Marrack, Howard Hughes Medical Institute, National Jewish Health, Denver, CO, and approved March 27, 2013 (received for review October 24, 2012)

Immunoresponsive gene 1 (*Irg1*) is highly expressed in mammalian macrophages during inflammation, but its biological function has not yet been elucidated. Here, we identify *Irg1* as the gene coding for an enzyme producing itaconic acid (also known as methylenesuccinic acid) through the decarboxylation of *cis*-aconitate, a tricarboxylic acid cycle intermediate. Using a gain-and-loss-of-function approach in both mouse and human immune cells, we found *Irg1* expression levels correlating with the amounts of itaconic acid, a metabolite previously proposed to have an antimicrobial effect. We purified IRG1 protein and identified its *cis*-aconitate decarboxylating activity in an enzymatic assay. Itaconic acid is an organic compound that inhibits isocitrate lyase, the key enzyme of the glyoxylate shunt, a pathway essential for bacterial growth under specific conditions. Here we show that itaconic acid inhibits the growth of bacteria expressing isocitrate lyase, such as *Salmonella enterica* and *Mycobacterium tuberculosis*. Furthermore, *Irg1* gene silencing in macrophages resulted in significantly decreased intracellular itaconic acid levels as well as significantly reduced antimicrobial activity during bacterial infections. Taken together, our results demonstrate that IRG1 links cellular metabolism with immune defense by catalyzing itaconic acid production.

During inflammatory responses, activated peripheral macrophages and microglial cells, the resident immune cells in the central nervous system, produce an array of inflammatory cytokines and free radicals that are responsible for their antimicrobial activity (1). Depending on the pathogens and the cytokine environment, macrophages are able to acquire a large spectrum of different phenotypes having specific pro- or anti-inflammatory properties (2, 3). Similar observations have been made in microglial cells, where the pro- or anti-inflammatory states have been elicited by different cytokines or bacterial components (4). In this context, gene expression profiling studies of murine macrophages and microglial cells have identified immunoresponsive gene 1 (*Irg1*) as one of the most highly up-regulated genes under proinflammatory conditions, such as bacterial infections (5–9). Increased *Irg1* expression levels have also been detected in chicken spleen macrophages after infection with *Salmonella enterica* (10). Furthermore, it has been shown that IRG1 could play an important role in the susceptibility toward Marek disease virus (11). *Irg1* was originally identified as a 2.3-kb cDNA from a library synthesized from mRNA isolated from a murine macrophage cell line after LPS stimulation (12). *Irg1* is also highly expressed in the early events leading to implantation in the pregnant uterus (13, 14), the specific phase in which a high level of inflammatory cytokines are secreted by the endometrial cells as well as by cells of the immune system that are recruited to the site of implantation (15). Interestingly, Irg1 has been used to classify functional profiles of neurotoxic C-C chemokine receptor $9^{+}Irg1^{+}$ and neurosupportive C-X-C chemokine receptor $3^{+}Irg1^{-}$ microglia in vivo (16). Although no mitochondria targeting signal sequence could be identified in the IRG1 amino acid sequence, IRG1 protein has been reported to associate with mitochondria (6).

Taken together, these data indicate an important role of *Irg1* during immune response. Although expression levels of *Irg1* have been extensively studied, its cellular function has not been addressed and is unknown. Based on sequence homology, IRG1 has been classified into the MmgE/PrpD family (17), which contains some proteins for which enzymatic activities have been identified in microorganisms (18). To elucidate if mammalian IRG1 exhibits an enzymatic function, we performed siRNA-mediated silencing of its expression in various cell models under inflammatory conditions and performed a nontargeted metabolomics analysis to detect significantly affected metabolites. Based on this analysis, we were able to elucidate the function of IRG1 as an enzyme catalyzing the production of the antimicrobial metabolite itaconic acid by decarboxylating *cis*-aconitate.

Results and Discussion

IRG1 Function. To investigate whether IRG1 has a potential enzymatic function, we analyzed the metabolomics profile of siRNA-mediated *Irg1* silencing under LPS stimulation in RAW264.7 cells. We first confirmed that the silencing of *Irg1* resulted in an 80% decrease of *Irg1* mRNA level compared with nonspecific siRNA control (Fig. 1*A*). We detected very low levels of *Irg1* mRNA (17-fold less compared with LPS-activated cells) in nonactivated macrophages. After silencing of *Irg1* in RAW264.7 cells, we measured 260 intracellular metabolites and, of these, we found that 5 were significantly different compared with untreated RAW264.7 cells (Welch's t test, $P < 0.05$). Most strikingly, we observed that the metabolite most significantly affected by *Irg1* silencing was itaconic acid ($P = 2.5 \times 10^{-8}$). This metabolite was very recently discovered by Strelko and colleagues in LPS-activated macrophages (19). However, until now, the enzyme catalyzing its production has not been described. Based on our experiments, the silencing of *Irg1* elicited a 60% decrease of itaconic acid compared with control conditions (Fig. 1*A*). Only low levels of the metabolite (11.5-fold less compared with LPS-activated cells) were measured in resting macrophages. Having identified itaconic acid as the main affected metabolite by *Irg1* silencing, we performed an intracellular quantification of this compound and found a concentration of 3 mM in BV2 retroviral-immortalized microglia (BV-2) cells and

Author contributions: A.M., R.B., and K.H. designed research; A.M., T.C., J.G., A.P., N.R., O.G., T.B., A.W., A.T., A.R., M.B., C.L.L., and K.H. performed research; A.M., T.C., A.P., N.R., O.G., C.L.L., E.M., and K.H. analyzed data; and A.M. and K.H. wrote the paper.

The authors declare no conflict of interest.

This article is a PNAS Direct Submission.

Freely available online through the PNAS open access option.

[1]A.M. and T.C. contributed equally to this work.

[2]To whom correspondence should be addressed. E-mail: karsten.hiller@uni.lu.

This article contains supporting information online at www.pnas.org/lookup/suppl/doi:10.1073/pnas.1218599110/-/DCSupplemental.

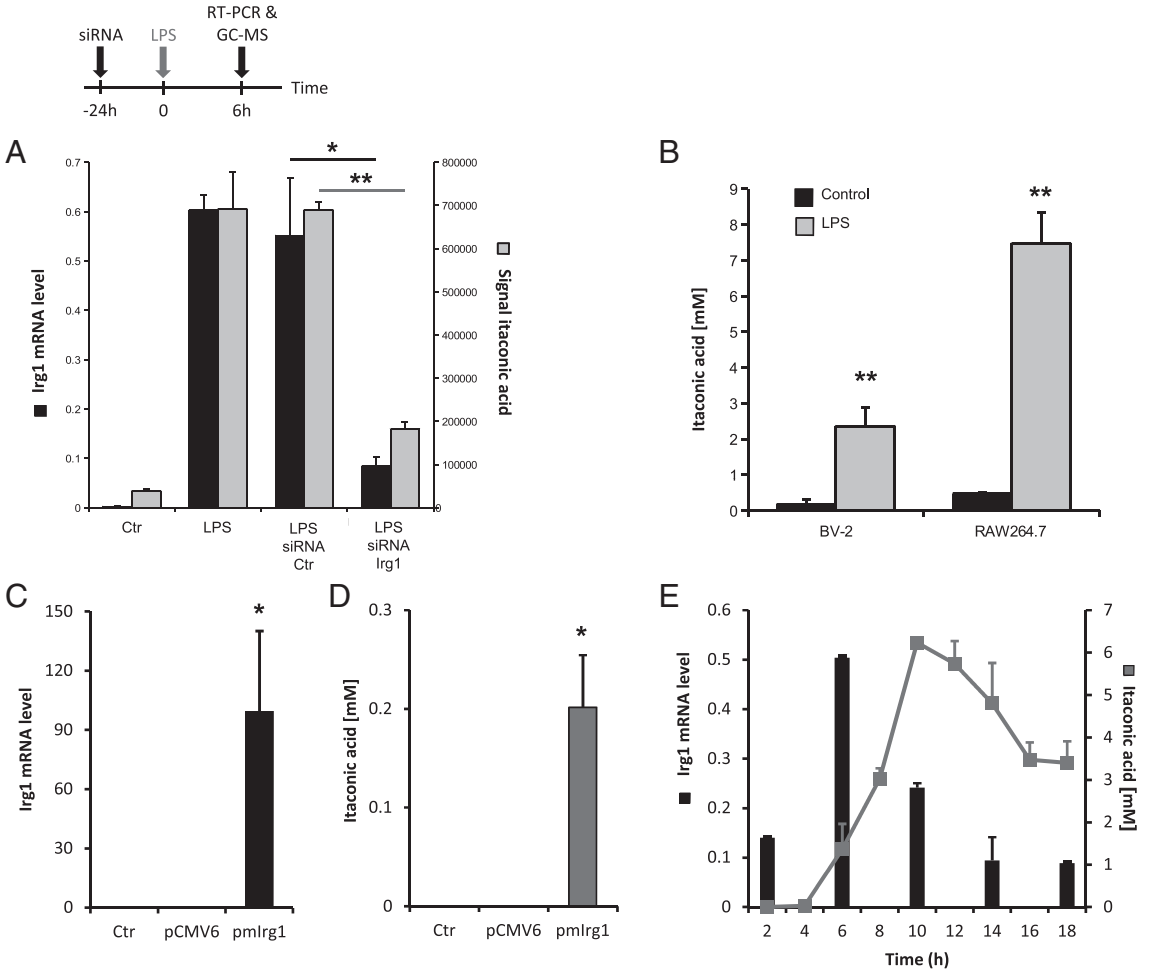

Fig. 1. (*A*) Levels of mRNA (left *y* axis, black bars) or itaconic acid (right *y* axis, gray bars) in resting (Ctr) or LPS-activated RAW264.7 macrophages transfected with either siRNA specific for *Irg1* or with siRNA Ctr. Metabolites and RNA extractions were performed after 6 h of stimulation. The levels of *Irg1* mRNA were determined by real-time RT-PCR and normalized using L27 as a housekeeping gene. Each bar represents the average expression fold change (± SD). The levels of itaconic acid were determined by GC/MS measurements. Each bar represents itaconic acid levels (± SD). $*P < 0.05$, $**P < 0.01$. (*B*) Itaconic acid quantification (mM) in mouse microglial cells (BV-2 cell line) and mouse macrophages (RAW264.7 cell line) after 6 h of LPS stimulation at 10 ng/mL (gray bars). Untreated cells were used as a control (black bars). Bars represent the mean of itaconic acid concentration (± SEM). $**P < 0.01$. Levels of mRNA (*C*) or itaconic acid (*D*) in human A549 lung cancer cells transfected with the mouse *Irg1* overexpressing plasmid (pm*Irg1*). Metabolites and RNA extractions were performed 24 h after transfection. Real-time RT-PCR results are normalized using L27 as a housekeeping gene and are shown as average expression fold change (± SEM). $*P < 0.05$, $**P < 0.01$. (*E*) RAW264.7 cells were treated with LPS (10 ng/mL) at different time points and analyzed for *Irg1* expression and itaconic acid concentration (mM).

8 mM in RAW264.7 mouse macrophages after LPS treatment (LPS 10 ng/mL) (Fig. 1*B*). We measured similar amounts in murine primary microglial cells induced by LPS treatment (Fig. S1). Such high intracellular itaconic acid concentrations after LPS treatment clearly point toward an immunological function of this metabolite.

To further study the metabolic activity of IRG1, we overexpressed murine *Irg1* in A549 human lung cancer cells. We found that these cells contained high amounts of both *Irg1* gene transcript and itaconic acid metabolite (0.2 ± 0.05 mM) 24 h after transfection, but not in nontransfected cells or in cells transfected with an empty control plasmid, in which *Irg1* mRNA and itaconic acid were below detection limit (Fig. 1 *C* and *D*).

Finally, to investigate the dynamics of *Irg1* expression and itaconic acid production after a proinflammatory stimulus, we analyzed RAW264.7 cells activated with LPS (10 ng/mL) at different time points. Although *Irg1* transcript was already produced after 2 h, significant amounts of itaconic acid could be measured starting 6 h after LPS treatment (Fig. 1*E*). The time-course of *Irg1* expression is in line with observed expression profiles of other proinflammatory cytokines. The positive time-dependent correlation between *Irg1* expression and itaconic acid levels further support the cellular role of IRG1 in itaconic acid production.

Itaconic Acid Metabolic Pathway. Intriguingly, murine IRG1 shows a 23% amino acid sequence identity to the enzyme *cis*-aconitate decarboxylase (CAD) expressed by the fungus *Aspergillus terreus* (Fig. S2). In fact, IRG1 is evolutionary conserved across a large set of species (Fig. S3). This fungus is commonly used for the biotechnological production of itaconic acid at an industrial scale (20). The biosynthesis of this dicarboxylic acid has been of interest because it can be used as a starting material for chemical synthesis of polymers (21). The fungal CAD enzyme catalyzes the formation of itaconic acid by decarboxylating *cis*-aconitate to itaconic acid (22). To determine if mammalian IRG1 has a similar function as CAD in *A. terreus*, we performed stable-isotope labeling experiments. We incubated LPS-activated RAW264.7 macrophages with uniformly ^{13}C-labeled glucose (U-$^{13}C_6$). Citrate synthase catalyzes the transfer of two labeled carbon atoms from acetyl-CoA to oxaloacetate resulting in M2 *cis*-aconitate

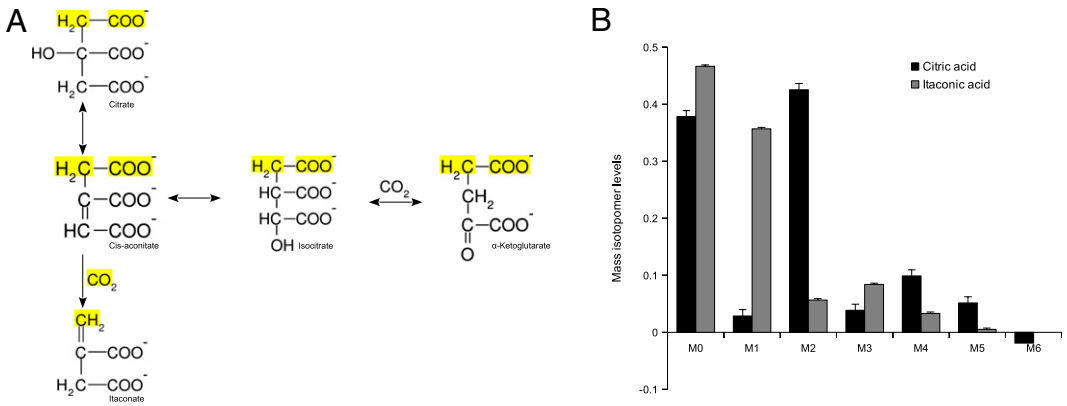

Fig. 2. (*A*) Synthesis pathway of itaconic acid in the TCA cycle. Itaconic acid can only contain one labeled carbon if produced in the first round of the TCA cycle (yellow-marked atoms). (*B*) Labeling of citric acid (black bars) and itaconic acid (gray bars) using glucose as a tracer in RAW264.7 macrophages. The major fraction of labeled itaconic acid contains one isotope, whereas citric acid contains mainly two labeled atoms.

isotopologues (Fig. 2*A*). If the decarboxylation is performed by a CAD homolog, the first carbon atom of the molecule is expected to be removed during the decarboxylation, resulting in M1 isotopologues of itaconic acid. In our experimental setting, we determined 45% of the citric acid molecules as M2 isotopologues, whereas 38% of the itaconic acid molecules were M1 isotopologues (Fig. 2*B*). We also found a significant fraction of M2, M3, and M4 itaconic acid isotopologues. The M4 fraction of itaconic acid reflects pyruvate carboxylase or reverse malic enzyme activity. Because of the symmetry of succinic acid, subsequent turns of the tricarboxylic acid (TCA) cycle can result in M2 or M3 isotopologues of itaconic acid.

The observations described so far strongly suggest that *Irg1* encodes a mammalian enzyme that catalyzes the decarboxylation of *cis*-aconitate to itaconic acid.

IRG1 Protein Purification and CAD Activity Assay. To directly demonstrate that the IRG1 protein catalyzes the decarboxylation of *cis*-aconitate, we purified FLAG-tagged IRG1 protein from human embryonic kidney 293T (HEK293T) cells transfected with a pCMV6-Entry-Irg1 expression plasmid. As depicted in Fig. 3*A*, protein extracts prepared from those cells catalyzed the conversion of *cis*-aconitate to itaconic acid. No itaconic acid formation was detected when extracts were prepared from cells transfected with an empty vector. Furthermore, affinity purification of the extract prepared from FLAG-Irg1 overexpressing cells clearly showed coelution of the *cis*-aconitate decarboxylase activity with a protein band identified as IRG1 by SDS/PAGE (expected molecular weight ~55 kDa for Flag-Irg1; Fig. 3*B*) and Western blot analysis using anti-IRG1 antibody (Fig. 3*C*). SDS/PAGE analysis showed that this purification procedure yielded a homogenous preparation of the IRG1 protein (Fig. 3*B*), demonstrating that the *cis*-aconitate decarboxylase activity measured in the purified fractions was not due to another contaminating protein.

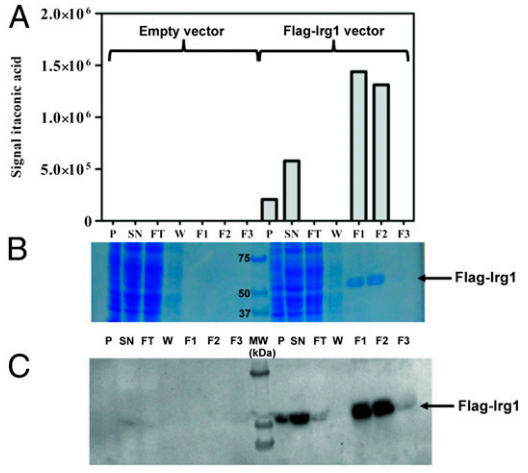

Fig. 3. Purification of *cis*-aconitate decarboxylase from HEK293T cells transfected with the pCMV6-Entry-Irg1 expression plasmid. (*A*) Extracts from cells transfected with empty plasmid or Flag-Irg1 plasmid were loaded onto an affinity resin (Cell MM2, FlagM purification kit, Sigma Aldrich) and proteins were eluted with Flag peptide. *Cis*-aconitate decarboxylase activity was measured in cell extracts and purification fractions as described in *Materials and Methods*. (*B*) A total of 12 μL of each protein fraction was loaded onto an SDS/PAGE gel that was stained with Coomassie Blue. (*C*) Western blot analysis of the same protein fractions was performed using an IRG1-specific antibody. F1-F3, elution fractions; FT, flow through; P, pellet; SN, supernatant; W, wash.

Itaconic Acid Is Produced by Human Primary Macrophages but at Lower Levels Compared with Mouse Cells. Because an *Irg1* homologous gene is annotated in the human genome on chromosome 13, we were interested to further analyze *IRG1* expression and itaconic acid amounts in human immune cells. To investigate this, we isolated $CD14^+$ primary human monocytes from the blood of different donors, cultured them for differentiation into macrophages for 11 d, and stimulated an inflammatory response with LPS (10 μg/mL) for 6 h. In line with our previous observations in mouse macrophages, we observed that *IRG1* expression in human peripheral blood mononuclear cell (PBMC)-derived macrophages was highly up-regulated after LPS activation compared with resting conditions in which *IRG1* mRNA levels were almost undetectable (Fig. 4*A*). Our results are in accordance with those of Roach and colleagues (23), who analyzed LPS-activated PBMCs' transcriptional profiles and observed *IRG1* up-regulation compared with control conditions. At the metabolite level, itaconic acid amounts were highly increased under LPS-induced inflammatory conditions compared with resting cells in which the metabolite was measured in low amounts or below the detection limits (Fig. 4*B*). In line with the induction of itaconic acid production, we observed elevated *IRG1* expression (Fig. 4 *C* and *D*). A similar trend was also mirrored by the expression of TNF-α mRNA, indicating that macrophages were activated (Fig. S4). Compared with the intracellular itaconic acid concentration in mouse immune cells, the concentration in human macrophages was two orders of magnitudes lower (8 mM vs. ~60 μM).

A major difference between mouse and human is the elevated production of NO in mouse macrophages under inflammatory conditions (24). It is well known that NO inhibits aconitase, the

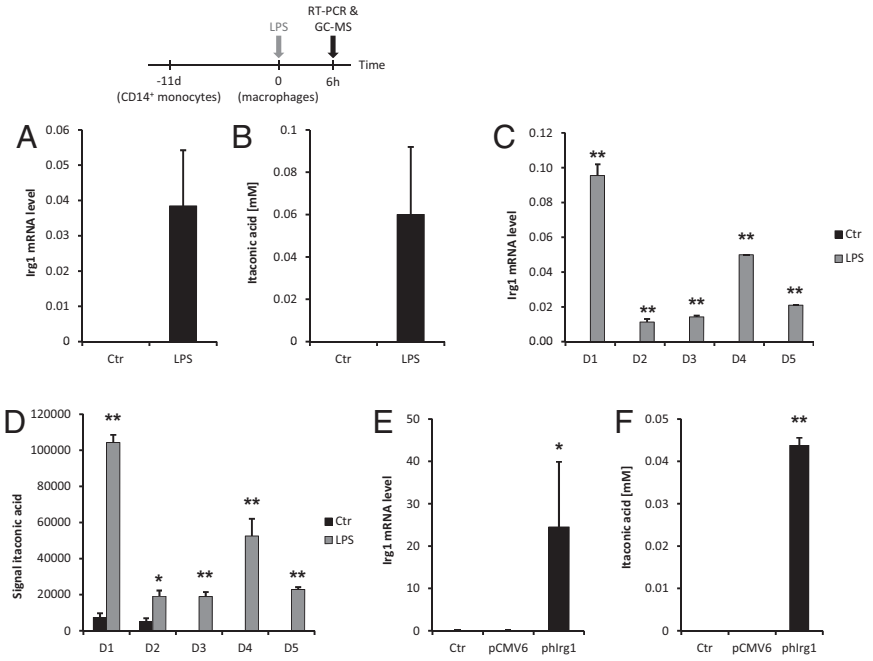

Fig. 4. Human *IRG1* expression and itaconic acid production. Levels of mRNA and itaconic acid in resting (Ctr) and LPS-activated (10 μg/mL) PBMC-derived macrophages. RNA and metabolites extractions were performed after 6 h of stimulation. (*A*) The levels of *IRG1* mRNA were determined by real-time RT-PCR and normalized using L27 as a housekeeping gene. Each bar represents the average expression fold change of five different donors (± SEM). (*B*) The corresponding levels of itaconic acid were determined by GC/MS measurements. Each bar represents itaconic acid levels (± SEM). $*P < 0.05$, $**P < 0.01$. (*C* and *D*) Differential *IRG1* gene expression analysis and itaconic acid production between five different donors. (*E* and *F*) Levels of mRNA (*E*) or itaconic acid (*F*) in human A549 lung cancer cells transfected with the human *IRG1* overexpressing plasmid (phIrg1). Metabolites and RNA extractions were performed 24 h after transfection. Real-time RT-PCR results are normalized using L27 as a housekeeping gene and are shown as average expression fold change (± SEM). $*P < 0.05$, $**P < 0.01$.

enzyme producing the itaconic acid precursor *cis*-aconitate (25–27). To test whether the NO-mediated inhibition of aconitase has an effect on itaconic acid production, we silenced the inducible nitric oxide synthetase (*iNOS*) gene to decrease NO levels in mouse macrophage (Fig. S5 *A* and *B*). On the other hand, we treated human PBMC-derived macrophages with the intracellular NO donor, diethylamine NONOate (28), to elevate the NO level in these cells (Fig. S6 *A–C*). We could not detect any effect on intracellular itaconic acid levels in either case. Based on these results, we assume that aconitase is not a rate-limiting step for itaconic acid synthesis.

Finally, we transfected A549 human lung cancer cells with a pCMV6 plasmid expressing human *IRG1* cDNA (phIrg1) to show CAD activity of human IRG1. We observed high amounts of both *IRG1* gene transcript and itaconic acid (0.044 ± 0.0018 mM) 24 h posttransfection (Fig. 4 *E* and *F*).

In Vivo *Irg1* Expression and Itaconic Acid Production. To confirm *Irg1* expression and itaconic acid production in vivo, we intraperitoneally injected C57BL/6 mice with LPS (1 mg/kg) and harvested the peritoneal macrophages after 24 h. We were able to measure high *Irg1* mRNA expression levels correlating with high amounts of intracellular itaconic acid compared with the saline-injected mice (Fig. 5 *A* and *B*).

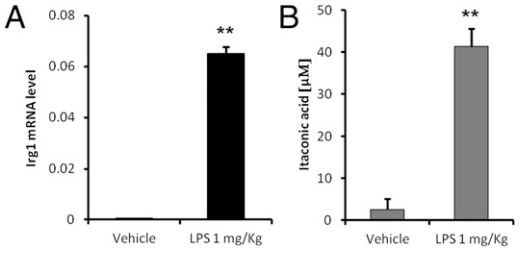

Fig. 5. Mouse peritoneal macrophages from eight saline- and seven LPS-injected mice (1 mg/kg) were isolated and pooled 24 h after i.p. injection. (*A*) *Irg1* expression levels and (*B*) itaconic acid production were analyzed compared with intraperitoneally saline-injected mice. Bars represent the mean of three technical replicates (± SEM).

Itaconic Acid Inhibits Bacterial Growth and Contributes to Antimicrobial Activity of Mouse Macrophages. It has previously been shown that itaconic acid has an antimicrobial activity by inhibiting isocitrate lyase (ICL) (29, 30), an enzyme of the glyoxylate shunt (Fig. 6*A*). The glyoxylate shunt is not present in animals, but is essential for the survival of bacteria growing on fatty acids or acetate as the limiting carbon source (31). The strategy for survival during chronic stages of infection entails a metabolic shift in the bacteria's carbon source to C_2 substrates generated by β-oxidation of fatty acids (31). Under these conditions, glycolysis is decreased and the glyoxylate shunt is significantly up-regulated to allow anaplerotic maintenance of the TCA cycle and assimilation of carbon via gluconeogenesis (32). Highly elevated levels of ICL are observed in *Mycobacterium tuberculosis* grown on C_2 sources (33) and shortly after uptake into human macrophages (34). Furthermore, it has been shown that persistence of *M. tuberculosis* in macrophages and mice requires the glyoxylate shunt enzyme ICL (35). In fact, *M. tuberculosis* cannot persist in macrophages when both isoforms of *icl* are genetically knocked out (36). Because the glyoxylate shunt is exclusively found in prokaryotes, lower eukaryotes, and plants, it represents a unique target for drug development (37).

To confirm the antimicrobial effect of itaconic acid on bacterial replication (30), we cultured the pathogens *M. tuberculosis* and *S. enterica* (both known to synthesize ICL for biosynthesis through the glyoxylate shunt) in liquid minimal medium supplemented with acetate as the unique carbon source to force the bacterial metabolism to use the glyoxylate shunt.

We determined bacterial growth in this medium in the presence of increasing itaconic acid concentration and observed that the effective concentration of itaconic acid varies depending on the analyzed bacteria. The growth of *M. tuberculosis* in vitro was completely inhibited at 25–50 mM itaconic acid concentrations (Fig. 6*B*), whereas significant effects were already observed at 10 mM for *S. enterica* (Fig. 6*C*). To exclude secondary toxic effects of itaconic acid, we measured the growth of the bacteria on glycerol or glucose as a carbon source. In this case, bacterial metabolism does not rely on the glyoxylate shunt. Under these conditions, itaconic acid does not affect the bacterial growth (Figs. S7*A* and S8*A*). To further demonstrate the specificity of the antimicrobial activity of itaconic acid, we performed the same

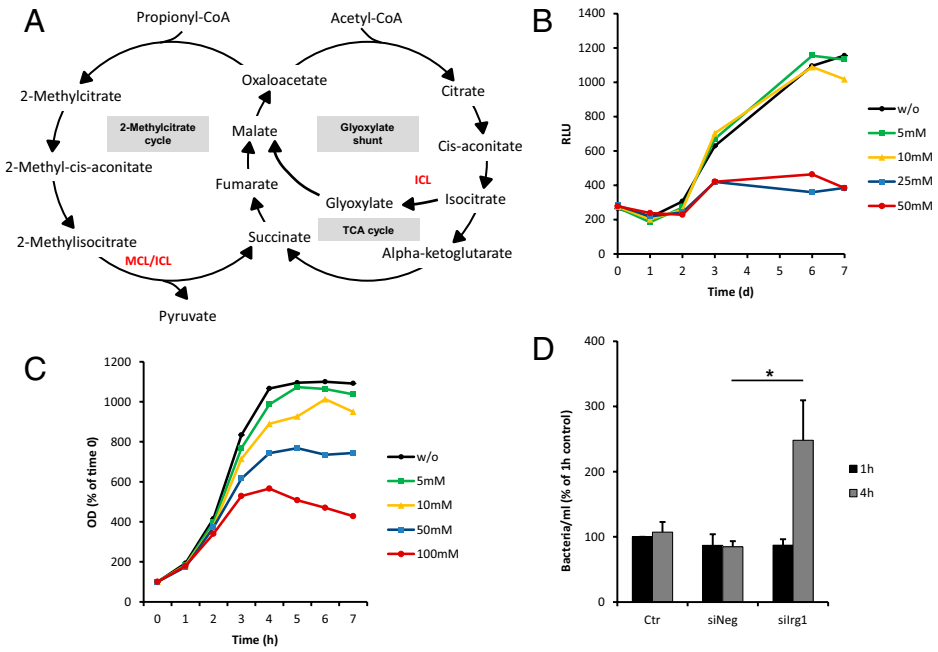

Fig. 6. Effect of itaconic acid on the bacterial growth. (*A*) Schematic of the glyoxylate shunt and the 2-methylcitrate cycle. (*B*) GFP-expressing *M. tuberculosis* bacteria were cultured in 7H9 medium supplemented with acetate, without (w/o) or with various concentrations of itaconic acid (5, 10, 25, 50 mM). Growth was measured as relative light units (RLU) at indicated time points. Curves represent the mean of three technical replicates. (*C*) *S. enterica* was grown in liquid medium with acetate, without (w/o) or in the presence of different concentrations of itaconic acid (5, 10, 50, 100 mM). The OD was measured every hour. Curves are calculated in percent relative to time 0 and represent the mean of three independent experiments. (*D*) RAW264.7 cells were transfected with either siRNA specific for *Irg1* (siIrg1) or with siRNA control (siNeg). After 24 h, the cells were infected with *S. enterica* at a multiplicity of infection of 1:10 and incubated for 1 h at 37 °C (*Materials and Methods*). Bars represent the mean of the numbers of bacteria per ml (± SEM) obtained from three independent experiments. $*P < 0.05$.

bacterial growth experiments, but by supplementing the medium with the itaconic acid precursor *cis*-aconitate. We observed that bacteria grown in the presence of *cis*-aconitate elicited an even more pronounced growth at different concentrations of this metabolite in both bacteria (Figs. S7 *B* and *C* and S8*B*), thus indicating that these bacteria started to use *cis*-aconitate as carbon source, in strong opposition with the effect we observed with itaconic acid.

It has been described that ICL exhibits additional methylisocitrate lyase (MCL) activity in *M. tuberculosis*. MCL is required for the detoxification of propionyl-CoA through the methylcitrate cycle (38, 39) (Fig. 6*A*). Propionyl-CoA accumulates during β-oxidation of odd-chain fatty acids and is produced from cholesterol of the host macrophages (40). As a result, inhibition of ICL in *M. tuberculosis* could have an additional toxic effect in the presence of propionate. To investigate the potential accentuated inhibition of the bacterial growth under these conditions, we incubated *M. tuberculosis* in glycerol with 0.1 μM propionate and increasing concentrations of itaconic acid. Indeed, the combination of these two effects inhibited *M. tuberculosis* growth at 5–10 mM of itaconic acid (Fig. S7*D*), thus confirming that MCL activity of ICL is affected by the metabolite.

To further investigate the involvement of itaconic acid in the antimicrobial activity of macrophages, we infected RAW264.7 cells with *S. enterica* and consequently observed an increased *Irg1* expression associated with high intracellular amounts of itaconic acid (Fig. S9 *A* and *B*). We saw that silencing of *Irg1* gene expression resulted in a decrease of intracellular itaconic acid concentration (Fig. S9*B*). We detected a significantly larger number of intracellularly viable bacteria in macrophages treated with siRNA targeting *Irg1* compared with those treated with an unspecific control siRNA or with siRNA targeting murine aconitase 2 (*Aco2*) 4 h after infection (Fig. 6*D* and Fig. S10).

Taken together, our results clearly demonstrate the importance of *Irg1* expression in macrophages during bacterial infection, thus contributing to their antimicrobial armature.

Conclusion

In this study, we report that the *Irg1* gene encodes an enzyme synthesizing itaconic acid from the TCA cycle intermediate *cis*-aconitate. We showed a strong up-regulation of both *Irg1* transcript and itaconic acid synthesis in macrophages in response to LPS activation. Furthermore, our data also show that IRG1-mediated itaconic acid production contributes to the antimicrobial activity of macrophages.

The discovery of an inducible enzyme linked to the TCA cycle and catalyzing the production of an antimicrobial metabolite is reminiscent of the mechanism found in the urea cycle responsible for the production of NO. iNOS is the enzyme that catalyzes the production of the antimicrobial compound NO from L-arginine (41) and, like IRG1, is induced in mouse macrophages and microglial cells under inflammatory conditions. In addition to other factors, NO and itaconic acid production by immune cells seem to represent an intrinsic property of these cells to self-react toward an inflammatory insult, and those metabolites seem to confer a form of innate metabolic immunity to macrophages and microglial cells.

Materials and Methods

Cell Culture. Primary human monocytic CD14+ cells were isolated in two steps from blood samples provided by Red Cross Luxembourg. First, (PBMCs were separated in 50-mL Leucoseptubes (Greiner) through Ficoll-Paque Premium (GE Healthcare) density-gradient centrifugation at 1,000 × *g* for 10 min at room temperature with no brake. Second, CD14+ cells were purified with magnetic labeling. Therefore, 2 μL of CD14 Microbeads (Miltenyi Biotech) per 10^7 PBMCs were incubated for 30 min at 4 °C followed by a positive LS column (Miltenyi Biotech) magnetic selection. The purified CD14+ cells were differentiated in six-well plates for 11 d in RPMI1640 medium without L-glutamine and phenol red (Lonza) supplemented with 10% (vol/vol) human serum (A&E Scientific), 1% (vol/vol) penicillin/streptomycin (Invitrogen), and 0.05% (vol/vol) L-glutamine (Invitrogen). The medium was changed on days 4 and 7.

Four cell lines, specifically murine microglial BV-2 cells (42), murine macrophages RAW264.7 (43) (ATCC TIB-71), human epithelial A549 lung cancer cells (44) (ATCC CCL-185), and human HEK293T cells (45) were used for the experiments.

Mouse i.p. Injection of LPS and Peritoneal Macrophages Isolation. All animal procedures, such as handling and euthanasia, have been performed according to the Federation of European Laboratory Animal Science Associations (FELASA) guidelines for the use of animals in research, and were institutionally approved by the Luxembourg Centre for System Biomedicine animal user committee and authorized by the local governmental agencies (Ministry of Health, Ministry of Agriculture, chief veterinarian of the Luxembourg government). Three-to-four-month-old SJL mice were injected i.p.

with LPS (1 mg/kg) or with saline vehicle and were deeply anesthetized after 24 h by i.p. injection of 50 mg/kg of ketamine·HCl and 5 mg/kg xylazine·HCl. Mice were then euthanized by cervical dislocation. Eight saline- and seven LPS-injected mice were used for peritoneal macrophages isolation. A small incision was made in the upper abdomen, and peritoneal macrophages were washed out with 4–5 mL ice-cold sterile PBS/mouse and pooled into falcon tubes. The cell suspension was pelleted in a cooled centrifuge for 5 min at 250 × g and the resulting pellet was worked up for metabolites and RNA extractions.

***M. tuberculosis* Growth Analysis.** GFP-expressing *M. tuberculosis* H37Rv bacteria (47) were generated using the plasmid 32362:pMN437 (Addgene), kindly provided by M. Niederweis (University of Alabama, Birmingham, AL) (48). 1×10^6 bacteria were cultured in 7H9 medium supplemented with different carbon sources as indicated in a total volume of 100 μL in a black 96-well plate with a clear bottom (Corning Inc) sealed with an air-permeable membrane (Porvair Sciences). Growth was measured as relative light units at 528 nm after excitation at 485 nm in a fluorescence microplate reader (Synergy 2, Biotek) at indicated time points.

Statistical Analysis. For comparison of means between two different treatments, the statistical analysis was done by the Student *t* test unless otherwise indicated. Error bars indicate SD or SEM as specified in the text.

For more information on protein purification and CAD activity assay, RNA isolation and RT-PCR, SDS/PAGE and Western blotting, GC/MS sample preparation and procedure as well as glucose labeling assay, please see *SI Materials and Methods*.

ACKNOWLEDGMENTS. We thank the laboratory of Prof. Paul Heuschling for mouse hosting, Prof. Stefan Ehlers for providing resources and facilitating interactions, and Lisa Niwinski for expert help and technical assistance. This study was supported by the Fonds National de la Recherche, Luxembourg (ATTRACT A10/03 and AFR 1328318).

1. David S, Kroner A (2011) Repertoire of microglial and macrophage responses after spinal cord injury. *Nat Rev Neurosci* 12(7):388–399.
2. Martinez FO, Sica A, Mantovani A, Locati M (2008) Macrophage activation and polarization. *Front Biosci* 13:453–461.
3. Mantovani A, et al. (2004) The chemokine system in diverse forms of macrophage activation and polarization. *Trends Immunol* 25(12):677–686.
4. Michelucci A, Heurtaux T, Grandbarbe L, Morga E, Heuschling P (2009) Characterization of the microglial phenotype under specific pro-inflammatory and anti-inflammatory conditions: Effects of oligomeric and fibrillar amyloid-beta. *J Neuroimmunol* 210(1-2): 3–12.
5. Tangsudjai S, et al. (2010) Involvement of the MyD88-independent pathway in controlling the intracellular fate of Burkholderia pseudomallei infection in the mouse macrophage cell line RAW 264.7. *Microbiol Immunol* 54(5):282–290.
6. Degrandi D, Hoffmann R, Beuter-Gunia C, Pfeffer K (2009) The proinflammatory cytokine-induced IRG1 protein associates with mitochondria. *J Interferon Cytokine Res* 29(1):55–67.
7. Thomas DM, Francescutti-Verbeem DM, Kuhn DM (2006) Gene expression profile of activated microglia under conditions associated with dopamine neuronal damage. *FASEB J* 20(3):515–517.
8. Basler T, Jeckstadt S, Valentin-Weigand P, Goethe R (2006) Mycobacterium paratuberculosis, Mycobacterium smegmatis, and lipopolysaccharide induce different transcriptional and post-transcriptional regulation of the IRG1 gene in murine macrophages. *J Leukoc Biol* 79(3):628–638.
9. Gautam A, et al. (2011) Interleukin-10 alters effector functions of multiple genes induced by Borrelia burgdorferi in macrophages to regulate Lyme disease inflammation. *Infect Immun* 79(12):4876–4892.
10. Matulova M, et al. (2012) Characterization of chicken spleen transcriptome after infection with Salmonella enterica serovar Enteritidis. *PLoS ONE* 7(10):e48101.
11. Smith J, et al. (2011) Systems analysis of immune responses in Marek's disease virus-infected chickens identifies a gene involved in susceptibility and highlights a possible novel pathogenicity mechanism. *J Virol* 85(21):11146–11158.
12. Lee CG, Jenkins NA, Gilbert DJ, Copeland NG, O'Brien WE (1995) Cloning and analysis of gene regulation of a novel LPS-inducible cDNA. *Immunogenetics* 41(5):263–270.
13. Cheon YP, Xu X, Bagchi MK, Bagchi IC (2003) Immune-responsive gene 1 is a novel target of progesterone receptor and plays a critical role during implantation in the mouse. *Endocrinology* 144(12):5623–5630.
14. Chen B, Zhang D, Pollard JW (2003) Progesterone regulation of the mammalian ortholog of methylcitrate dehydratase (immune response gene 1) in the uterine epithelium during implantation through the protein kinase C pathway. *Mol Endocrinol* 17(11):2340–2354.
15. Mor G, Cardenas I, Abrahams V, Guller S (2011) Inflammation and pregnancy: The role of the immune system at the implantation site. *Ann N Y Acad Sci* 1221:80–87.
16. Li H, et al. (2006) Different neurotropic pathogens elicit neurotoxic CCR9- or neurosupportive CXCR3-expressing microglia. *J Immunol* 177(6):3644–3656.
17. Lohkamp B, Bäuerle B, Rieger PG, Schneider G (2006) Three-dimensional structure of iminodisuccinate epimerase defines the fold of the MmgE/PrpD protein family. *J Mol Biol* 362(3):555–566.
18. Kanamasa S, Dwiarti L, Okabe M, Park EY (2008) Cloning and functional characterization of the cis-aconitic acid decarboxylase (CAD) gene from Aspergillus terreus. *Appl Microbiol Biotechnol* 80(2):223–229.
19. Strelko CL, et al. (2011) Itaconic acid is a mammalian metabolite induced during macrophage activation. *J Am Chem Soc* 133(41):16386–16389.
20. Bentley R, Thiessen CP (1957) Biosynthesis of itaconic acid in Aspergillus terreus. I. Tracer studies with C14-labeled substrates. *J Biol Chem* 226(2):673–687.
21. Okabe M, Lies D, Kanamasa S, Park EY (2009) Biotechnological production of itaconic acid and its biosynthesis in Aspergillus terreus. *Appl Microbiol Biotechnol* 84(4): 597–606.
22. Bonnarme P, et al. (1995) Itaconate biosynthesis in Aspergillus terreus. *J Bacteriol* 177(12):3573–3578.
23. Roach JC, et al. (2007) Transcription factor expression in lipopolysaccharide-activated peripheral-blood-derived mononuclear cells. *Proc Natl Acad Sci USA* 104(41):16245–16250.
24. Schroder K, et al. (2012) Conservation and divergence in Toll-like receptor 4-regulated gene expression in primary human versus mouse macrophages. *Proc Natl Acad Sci USA* 109(16):E944–E953.
25. Gardner PR, Costantino G, Szabó C, Salzman AL (1997) Nitric oxide sensitivity of the aconitases. *J Biol Chem* 272(40):25071–25076.
26. Drapier JC, Hibbs JB, Jr. (1996) Aconitases: A class of metalloproteins highly sensitive to nitric oxide synthesis. *Methods Enzymol* 269:26–36.
27. Stadler J, et al. (1991) Effect of exogenous and endogenous nitric oxide on mitochondrial respiration of rat hepatocytes. *Am J Physiol* 260(5 Pt 1):C910–C916.
28. Kovaleva V, Berezhnaya E, Komandirov M, Rudkovskii M, Uzdensky A (2013) Involvement of nitric oxide in photodynamic injury of neurons and glial cells. *Nitric Oxide* 29:46–52.
29. Patel TR, McFadden BA (1978) Caenorhabditis elegans and Ascaris suum: Inhibition of isocitrate lyase by itaconate. *Exp Parasitol* 44(2):262–268.
30. McFadden BA, Purohit S (1977) Itaconate, an isocitrate lyase-directed inhibitor in Pseudomonas indigofera. *J Bacteriol* 131(1):136–144.
31. Hillier S, Charnetzky WT (1981) Glyoxylate bypass enzymes in Yersinia species and multiple forms of isocitrate lyase in Yersinia pestis. *J Bacteriol* 145(1):452–458.
32. Sharma V, et al. (2000) Structure of isocitrate lyase, a persistence factor of Mycobacterium tuberculosis. *Nat Struct Biol* 7(8):663–668.
33. Höner Zu Bentrup K, Miczak A, Swenson DL, Russell DG (1999) Characterization of activity and expression of isocitrate lyase in Mycobacterium avium and Mycobacterium tuberculosis. *J Bacteriol* 181(23):7161–7167.
34. Hou JY, Graham JE, Clark-Curtiss JE (2002) Mycobacterium avium genes expressed during growth in human macrophages detected by selective capture of transcribed sequences (SCOTS). *Infect Immun* 70(7):3714–3726.
35. McKinney JD, et al. (2000) Persistence of Mycobacterium tuberculosis in macrophages and mice requires the glyoxylate shunt enzyme isocitrate lyase. *Nature* 406(6797): 735–738.
36. Muñoz-Elías EJ, McKinney JD (2005) Mycobacterium tuberculosis isocitrate lyases 1 and 2 are jointly required for in vivo growth and virulence. *Nat Med* 11(6):638–644.
37. Russell DG (2001) Mycobacterium tuberculosis: Here today, and here tomorrow. *Nat Rev Mol Cell Biol* 2(8):569–577.
38. Muñoz-Elías EJ, Upton AM, Cherian J, McKinney JD (2006) Role of the methylcitrate cycle in Mycobacterium tuberculosis metabolism, intracellular growth, and virulence. *Mol Microbiol* 60(5):1109–1122.
39. Savvi S, et al. (2008) Functional characterization of a vitamin B12-dependent methylmalonyl pathway in Mycobacterium tuberculosis: Implications for propionate metabolism during growth on fatty acids. *J Bacteriol* 190(11):3886–3895.
40. Russell DG, et al. (2010) Mycobacterium tuberculosis wears what it eats. *Cell Host Microbe* 8(1):68–76.
41. Knowles RG, Moncada S (1994) Nitric oxide synthases in mammals. *Biochem J* 298 (Pt 2):249–258.
42. Bocchini V, et al. (1992) An immortalized cell line expresses properties of activated microglial cells. *J Neurosci Res* 31(4):616–621.
43. Raschke WC, Baird S, Ralph P, Nakoinz I (1978) Functional macrophage cell lines transformed by Abelson leukemia virus. *Cell* 15(1):261–267.
44. Giard DJ, et al. (1973) In vitro cultivation of human tumors: Establishment of cell lines derived from a series of solid tumors. *J Natl Cancer Inst* 51(5):1417–1423.
45. Graham FL, Smiley J, Russell WC, Nairn R (1977) Characteristics of a human cell line transformed by DNA from human adenovirus type 5. *J Gen Virol* 36(1):59–74.
46. Smal C, et al. (2006) Identification of in vivo phosphorylation sites on human deoxycytidine kinase. Role of Ser-74 in the control of enzyme activity. *J Biol Chem* 281(8): 4887–4893.
47. Steinhäuser C, et al. (2013) Lipid-labeling facilitates a novel magnetic isolation procedure to characterize pathogen-containing phagosomes. *Traffic* 14(3):321–336.
48. Song H, Sandie R, Wang Y, Andrade-Navarro MA, Niederweis M (2008) Identification of outer membrane proteins of Mycobacterium tuberculosis. *Tuberculosis (Edinb)* 88(6):526–544.

Supporting Information

Michelucci et al. 10.1073/pnas.1218599110

SI Materials and Methods

Cell Transfections. The ON-TARGETplus SMARTpool containing four different siRNA sequences, all specific to murine *Irg1* (siRNA *Irg1*), murine iNOS (siRNA iNOS), murine aconitase 2 (siRNA *Aco2*), and the corresponding nontargeting control (siRNA Ctr), were designed and synthesized by Thermo Scientific Dharmacon.

RAW264.7 macrophages were transfected with Amaxa 4D-Nucleofector Device (Lonza) using the Amaxa SG cell line 4D Nucleofector Kit for THP-1 cells according to the manufacturer's instructions.

Briefly, transfection with siRNA complexes was carried out from pelleted and resuspended cells (1×10^6 cells per condition). Transfection reagent and siRNA were prepared according to manufacturer's instructions (Amaxa). siRNAs were added at a final concentration of 100 nM. After the nucleofection processing using "RAW264.7 (ATCC) program" on the Nucleofection device, the cells were seeded at a density of 1×10^6 cells per well in 12-well plates in DMEM supplemented with 10% FBS and incubated for 24 h.

pCMV6-Irg1 overexpressing plasmid (4 μg, *Mus musculus* immune responsive gene 1 transfection-ready DNA, OriGene), in parallel with the empty plasmid (4 μg), was transfected into 1.5×10^6 A549 cells using Lipofectamine 2000 (Invitrogen) and further incubated for 24 h. pCMV6-Entry-Irg1 plasmid was transfected into HEK293T cells by the jetPEI procedure as described previously (46) and further incubated for 48 h before extraction.

Macrophages Bacterial Phagocytosis and Killing Assay. Untransfected or transfected RAW264.7 macrophages (with unspecific siRNA, *Irg1*-specific siRNA or mitochondrial aconitase-specific siRNA) were seeded at a density of 25×10^4 per well in 48-well plates in 250 μL DMEM complemented with 10% FBS at 37 °C with 5% CO_2. After 24 h, the cells were infected with *S. enterica* serovar typhimurium at a multiplicity of infection of 1:10 (one bacteria per 10 macrophages) or 1:1 (one bacteria per one macrophage) and incubated for 1 h at 37 °C with 5% CO_2. Macrophages were then washed with sterile PBS and resuspend in DMEM complemented with 10% FBS and 100 μg/mL gentamicin to kill noningested bacteria and further incubated for 1 h (this was considered as time point 0 h) or 4 h (time point 4 h) at 37 °C with 5% CO_2. After washing with sterile PBS, macrophages were disrupted for 15 min with 250 μL dH_2O to release intracellular bacteria. The amount of viable intracellular bacteria was determined by plating on Luria-Bertani agar plates using four dilutions from 1:10 up to 1:10,000 and incubation overnight at 37 °C. For metabolite extraction, macrophages were seeded at a density of 75×10^4 per well in 12-well plates. Intracellular metabolites were extracted and mRNA isolated at time point 0 h and time point 4 h for GC/MS measurements and RT-PCR, respectively. All conditions were performed in technical triplicates.

Protein Purification and CAD Activity Assay. HEK293T cells were extracted 48 h after transfection by scraping them into a lysis buffer containing 25 mM Hepes, pH 7.1, and 1× protease inhibitor mixture (Roche). After two freeze/thaw cycles, cell extracts were incubated for 30 min on ice in the presence of DNase I (200 U/mL extract; Roche Applied Science) and 10 mM $MgSO_4$. The crude cell extracts were centrifuged for 5 min at 16,000 × *g* (4 °C) and pellets were resuspended in lysis buffer for SDS/PAGE analysis. Flag-Irg1 was purified from the supernatant using the FlagM purification kit, according to the manufacturer's instructions (Sigma Aldrich). About 3 mg protein were loaded onto 250 μL anti-Flag affinity resin and retained proteins were eluted with a solution containing 200 μg/mL Flag peptide (3 × 400 μL fractions). Protein purity was checked by SDS/PAGE analysis. Protein concentration was measured by the Bradford assay using Bradford reagent (Bio-Rad).

Cis-aconitate decarboxylase activity was measured by incubating cell extracts or purified protein fractions (10 μL) at 30 °C and for 40 min in a reaction mixture containing 25 mM Hepes, pH 7.1, and 1 mM *cis*-aconitate in a total volume of 100 μL. Reactions were stopped by addition of 900 μL methanol/water (8:1) mix. After 10 min centrifugation at 16,100 × *g* and 4 °C, 100 μL of the supernatant were collected and evaporated under vacuum at −4 °C using a refrigerated CentriVapConcentrator (Labconco).

RNA Isolation and RT-PCR. Total RNA was purified from cultured cells using the Qiagen RNeasy Mini Kit (Qiagen) per manufacturer's instructions. First-strand cDNA was synthesized from 0.5 to 2 μg of total RNA using SuperScript III (Invitrogen) with 1 μL (50μM)/reaction oligo$(dT)_{20}$ as primer. Individual 20 μL SYBR Green real-time PCR reactions consisted of 2 μL of diluted cDNA, 10 μL of 2× iQ SYBR Green Supermix (Bio-Rad), and 0.5 μL of each 10 μM optimized forward and reverse primers in 7 μL RNase-free water. Primer sequences designed using Beacon Designer software (Bio-Rad), provided by Eurogentec, or directly designed by Thermo Scientific, are available on request. For the human Irg1 primers, the NCBI/Primer-BLAST tool available at http://www.ncbi.nlm.nih.gov/tools/primer-blast/ was used. The PCR was carried out on a Light Cycler 480 (Roche Diagnostics), using a three-stage program provided by the manufacturer: 10 min at 95 °C and 40 cycles of 30 s at 95 °C, 30 s at 60 °C, and 30 s at 72 °C followed by 10-s 70–95° melting curves. All experiments included three no-template controls and were performed on three biological replicates with three technical replicates for each sample. For standardization of quantification, L27 was amplified simultaneously.

SDS/PAGE and Western Blotting Analysis. Heat-denatured protein samples were separated on 10% SDS-polyacrylamide gels electrophoresis followed by transfer to nitrocellulose membranes 0.2 μm (Sigma). After blocking with 5% (wt/vol) dry milk in PBS, the membrane was incubated overnight at 4 °C in primary anti-Irg1 antibody from rabbit (Sigma) diluted 1:500 in 1% BSA/PBS with constant shaking. After three washing steps with PBS containing 0.1% Tween-20, the membrane was incubated with anti-rabbit antibody coupled to horseradish peroxidase and revealed by chemiluminescence using the Amersham ECL detection reagents (GE Healthcare).

GC/MS Sample Preparation and Procedure. Cells grown in six-well plates were washed with 1 mL saline solution and quenched with 0.4 mL −20 °C methanol. After adding an equal volume of 4 °C cold water, cells were collected with a cell scraper and transferred in tubes containing 0.4 mL −20 °C chloroform. The extracts were vortexed at 1,400 rpm for 20 min at 4 °C and centrifuged at 16,000 × *g* for 5 min at 4 °C. 0.3 mL of the upper aqueous phase was collected in specific GC glass vials and evaporated under vacuum at −4 °C using a refrigerated CentriVap Concentrator (Labconco). The metabolite extractions of cells grown on 12-well plates were performed using half of the volumes.

The interphase was centrifuged with 1 mL −20 °C methanol at 16,000 × *g* for 5 min at 4 °C. The pellet was used for RNA isolation.

Metabolite derivatization was performed using an Agilent Autosampler. Dried polar metabolites were dissolved in 15 μL of 2% methoxyamine hydrochloride in pyridine at 45 °C. After 30 min, an equal volume of 2,2,2-trifluoro-*N*-methyl-*N*-trimethylsilyl-acetamide + 1% chloro-trimethyl-silane were added and held for 30 min at 45 °C. Metabolites extracted out of 12-well plates were derivatized using half of the reagent volumes. GC/MS analysis is described in *SI Materials and Methods*, *GC/MS Analysis*.

Glucose Labeling Assay. RAW264.7 macrophages were seeded at a density of 1×10^6 per well in 12-well plates in DMEM supplemented with 10% FBS and 1% penicillin/streptomycin at 37 °C with 5% CO_2. After 24 h, the medium was changed to DMEM containing uniformly labeled 25 mM [U-^{13}C] glucose (Cambridge Isotope). Simultaneously, the cells were activated with 10 ng/mL LPS. After 6 h of incubation, the metabolites were extracted.

***S. enterica* Growth Analysis.** *S. enterica* serovar typhimurium bacteria were grown in liquid medium as detailed in the text in the presence different concentrations of itaconic acid or *cis*-aconitate (5, 10, 50, 100 mM). Growth was measured as OD at indicated time points.

Mice. All animal procedures have been performed according to the European Guidelines for the use of animals in research (86/609/CEE). All efforts were made to minimize suffering. All animals have been raised and crossed in an indoor animal house in a 12-h light/dark cycle and have been provided with water and food ad libitum.

Cell Culture. Mixed glial cell cultures were prepared from the brains of newborn C57BL/6 mice. After carefully removing meninges and large blood vessels, the brains were pooled and then minced in cold PBS solution. The tissue was mechanically dissociated with Pasteur pipettes and the resultant cell suspension was passed through a 21G hypodermic needle. After washes and centrifugations, the mixed glial cells were plated into poly-D-lysine (PDL, Sigma) coated six-well plates (two brains per six-well plate) in DMEM (Invitrogen) supplemented with 100 U/mL penicillin, 100 mg/mL streptomycin (Sigma), and 10% heat-inactivated FBS (Invitrogen) in a water-saturated atmosphere containing 5% CO_2 at 37 °C. The medium was replaced every 3–4 d. After 7–10 d, when the cultures reached confluence, microglia were detached by a 30-min shaking on a rotary shaker (180 rpm). Detached cells, mainly microglia (>95%), were then plated in multiwell plates in conditioned medium and further incubated for 3 d.

BV2 retroviral-immortalized microglia (BV-2), human embryonic kidney 293T (HEK293T), and RAW264.7 cell lines were maintained in DMEM with or without sodium pyruvate, supplemented with 10% heat-inactivated FBS (South American, Invitrogen). No antibiotics were used for BV-2; 1% penicillin/streptomycin were used for RAW264.7 and HEK293T cells.

A549 cells were cultivated in DMEM without sodium pyruvate and supplemented with 10% heat-inactivated FBS and 1% penicillin/streptomycin. Cells were grown and maintained according to standard cell culture protocols and kept at 37 °C with 5% CO_2.

For experiments, BV-2, RAW264.7, and A549 cells were seeded into multiwell plates at a density of 0.5×10^5 (BV-2) and 1.0×10^5 (RAW264.7 and A549) cells/well (six-well plates). After 3 d of culture, the cells were activated adding specific stimuli to the culture medium.

LPS 055:B5 from *Escherichia coli* (Sigma) was added at specified time points and at different doses in mouse primary microglia (1 ng/mL), BV-2, and RAW264.7 (10 ng/mL) or peripheral blood mononuclear cell (PBMC)-derived macrophages (10 μg/mL) to obtain similar activation states because of the differences in sensitivity between murine primary cultures and cell lines as well as between mouse and human cells.

GC/MS Analysis. GC/MS analysis was performed using an Agilent 6890 GC equipped with a 30 m DB-35MS capillary column. The GC was connected to an Agilent 5975C MS operating under electron impact ionization at 70 eV. The MS source was held at 230 °C and the quadrupole at 150 °C. The detector was operated in scan mode and 1 μL of derivatized sample was injected in splitless mode. Helium was used as carrier gas at a flow rate of 1 mL/min. The GC oven temperature was held at 80 °C for 6 min and increased to 300 °C at 6 °C/min. After 10 min, the temperature was increased to 325 °C at 10 °C/min for 4 min. The run time of one sample was 59 min.

NO Donor Treatments. Human PBMCs were seeded and differentiated into macrophages as described previously. Diethylamine NONOate (DEA NONOate, Sigma), an intracellular NO donor, was added at different concentrations (1, 10, 100 μM) alone or together with LPS (100 μg/mL). After 12 h of incubation, the metabolites were extracted.

Griess Nitrite Assay. After 12 h, 180 μL of medium was harvested and combined with 20 μL of 1 mM NaOH on ice to stop the dissociation reaction. Levels of nitrite formed from the reaction with H_2O were determined using the Griess assay. In brief, 50 μL of medium sample or nitrite ion chromatographic (IC) standard (Sigma) was pipetted in triplicate in a 96-well plate. To each well, equal volumes of 1× Griess Reagent (Sigma) were added. Absorbance was read at 540 nm and nitrite concentrations were calculated.

Sequence Alignment. Multiple sequence alignment of *Cis*-aconitic acid decarboxylase (*Aspergillus terreus*), immune-responsive gene 1 protein homolog (human), immune-responsive gene 1 protein (mouse), and iminodisuccinate epimerase (*Agrobacterium tumefaciens*) was performed using MAFFT version 6 (1, 2) and visualized with ESPript (3). Sequences were obtained from UniProt Knowledgebase (UniProtKB) with the following accession numbers: B3IUN8 (CAD1), A6NK06 (IRG1 human), P54987 (IRG1 mouse), and Q1L4E3 (iminodisuccinate epimerase).

1. Katoh K, Toh H (2008) Recent developments in the MAFFT multiple sequence alignment program. *Brief Bioinform* 9(4):286–298.
2. Katoh K, Misawa K, Kuma K, Miyata T (2002) MAFFT: A novel method for rapid multiple sequence alignment based on fast Fourier transform. *Nucleic Acids Res* 30(14): 3059–3066.
3. Gouet P, Courcelle E, Stuart DI, Métoz F (1999) ESPript: Analysis of multiple sequence alignments in PostScript. *Bioinformatics* 15(4):305–308.

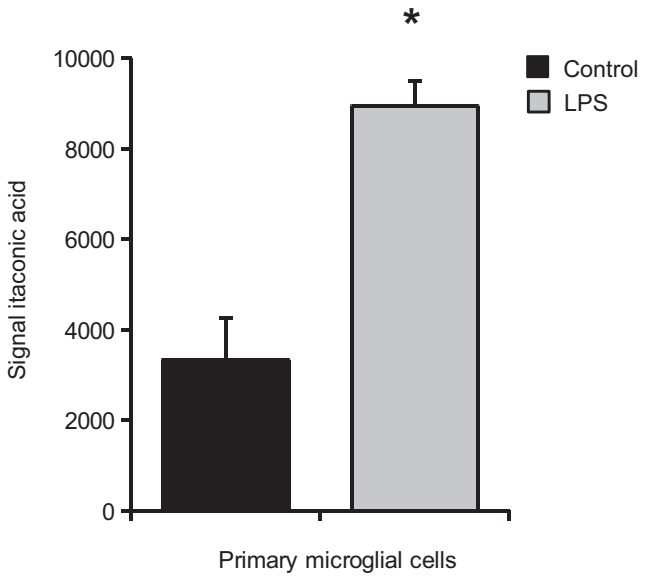

Fig. S1. Itaconic acid in mouse primary microglial cells. Primary microglial cells were treated for 6 h with LPS (1 ng/mL) (gray bars) or left untreated (black bars). Bars represent the mean of itaconic acid levels (± SD). *$P < 0.05$.

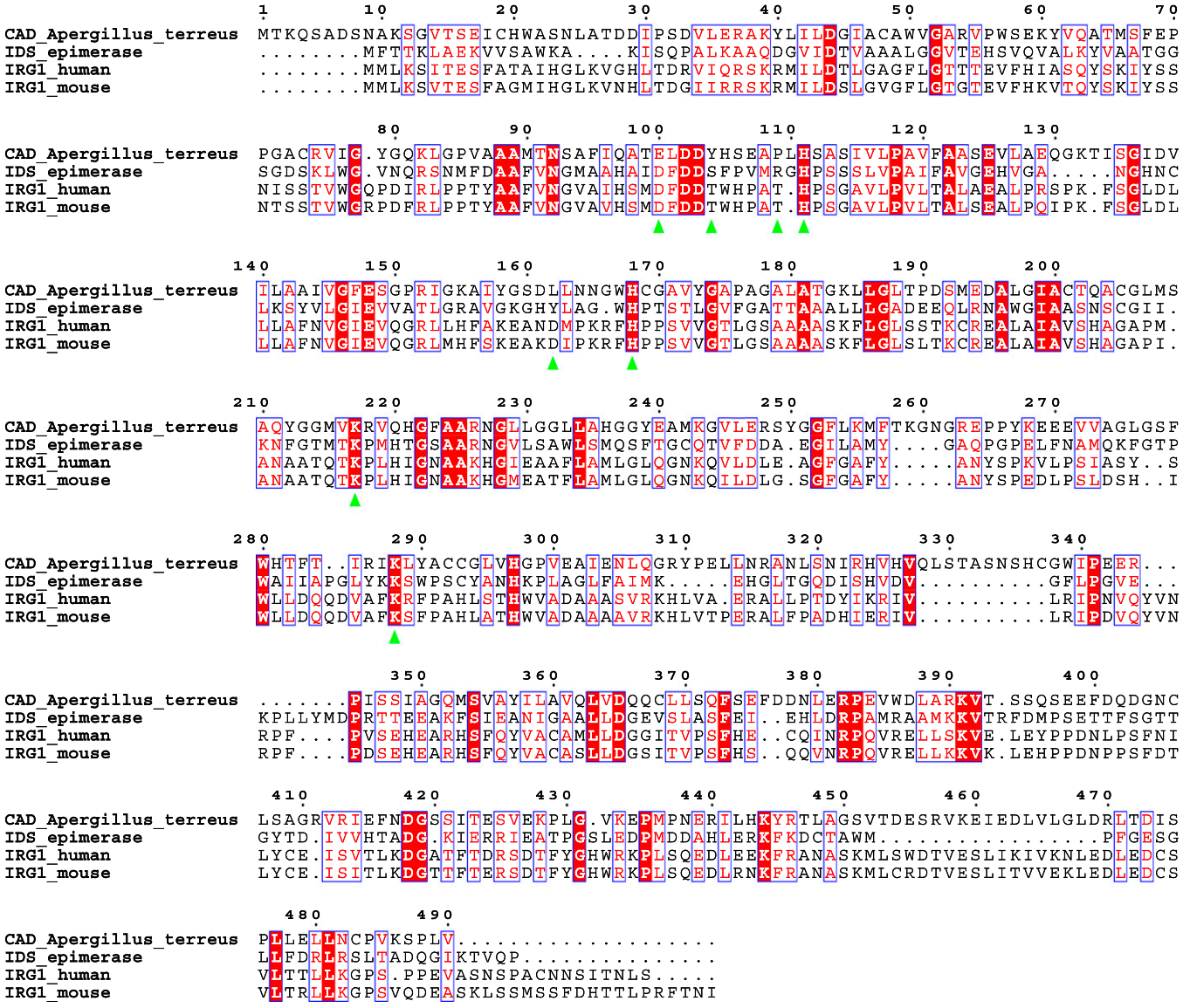

Fig. S2. Multiple sequence alignment of *cis*-aconitic acid decarboxylase (CAD) (*Aspergillus terreus*), immune-responsive gene 1 protein homolog (IRG1) (Homo sapiens), immune-responsive gene 1 protein (IRG1) (Mus musculus), and iminodisuccinate (IDS) epimerase (*Agrobacterium tumefaciens*). Between CAD1 and IRG1, five of eight active site residues are conserved. Conserved residues are shown in red; residues assumed to build active site are indicated with green triangles below the alignment. Figure was drawn with ESPript. Sequences were obtained from UniProt Knowledgebase (UniProtKB) with the following accession numbers: B3IUN8 (CAD1), A6NK06 (IRG1 human), P54987 (IRG1 mouse), and Q1L4E3 (IDS epimerase).

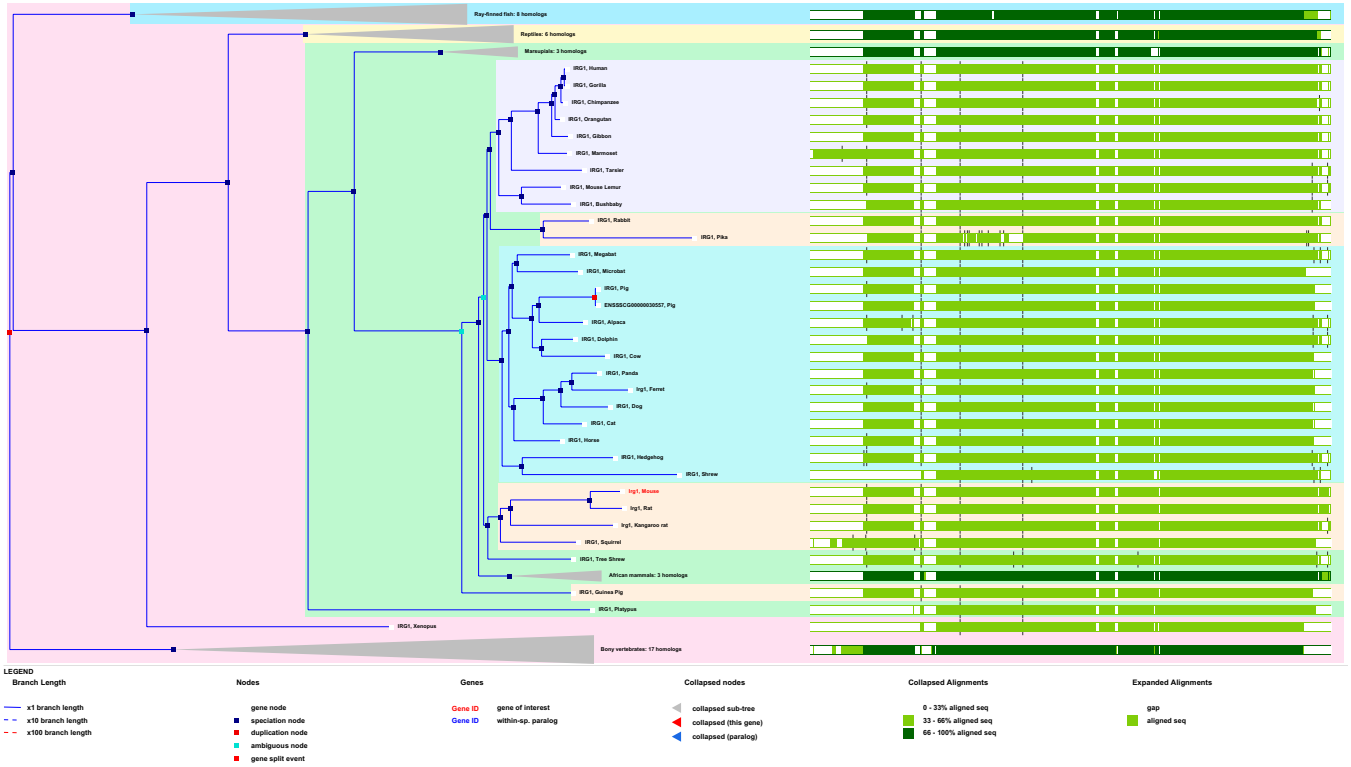

Fig. S3. Gene tree of mouse *Irg1*. Gene Tree was generated using the Ensembl gene orthology/paralogy prediction method pipeline (1). (*Left*) The evolutionary history of *Irg1* across species. (*Right*) A multiple sequence alignment of the associated proteins. Green bars show areas of amino acid alignment; white areas are gaps in the alignment.

1. Vilella AJ, et al. (2009) EnsemblCompara GeneTrees: Complete, duplication-aware phylogenetic trees in vertebrates. *Genome Res* 19(2):327–335.

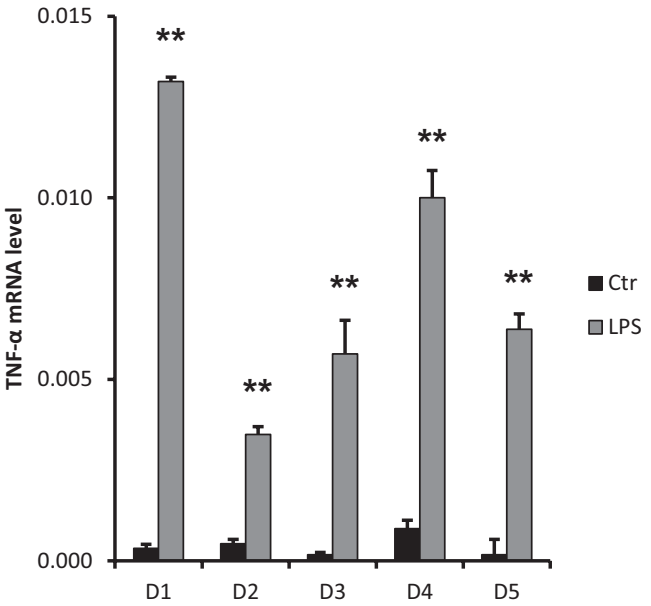

Fig. S4. TNF-α expression in LPS-activated human PBMC-derived macrophages. RNA extractions were performed after 6 h of LPS (10 μg/mL) stimulation of PBMC-derived macrophages from five different donors (D). The levels of TNF-α mRNA were determined by real-time RT-PCR and normalized using L27 as a housekeeping gene. Each bar represents the average expression fold change of three technical replicates (± SEM). $^{**}P < 0.01$.

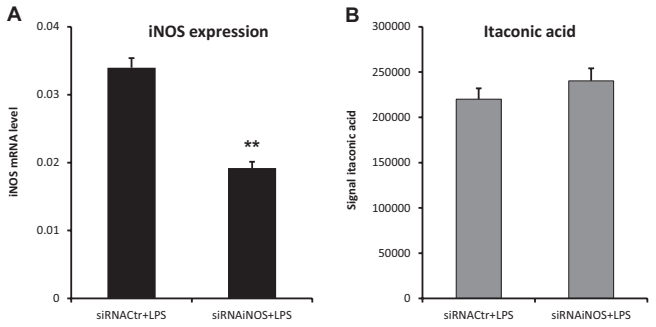

Fig. S5. (*A*) Levels of mRNA or (*B*) itaconic acid in LPS-activated RAW264.7 macrophages transfected with either siRNA specific for iNOS or with siRNA nontargeting control (Ctr). Metabolites and RNA extractions were performed after 6 h of stimulation. The levels of iNOS mRNA were determined by real-time RT-PCR and normalized using L27 as a housekeeping gene. Each bar represents the average expression fold change (± SEM) from three independent experiments. The levels of itaconic acid were determined by GC/MS measurements. Each bar represents itaconic acid levels (± SEM). $^{**}P < 0.01$.

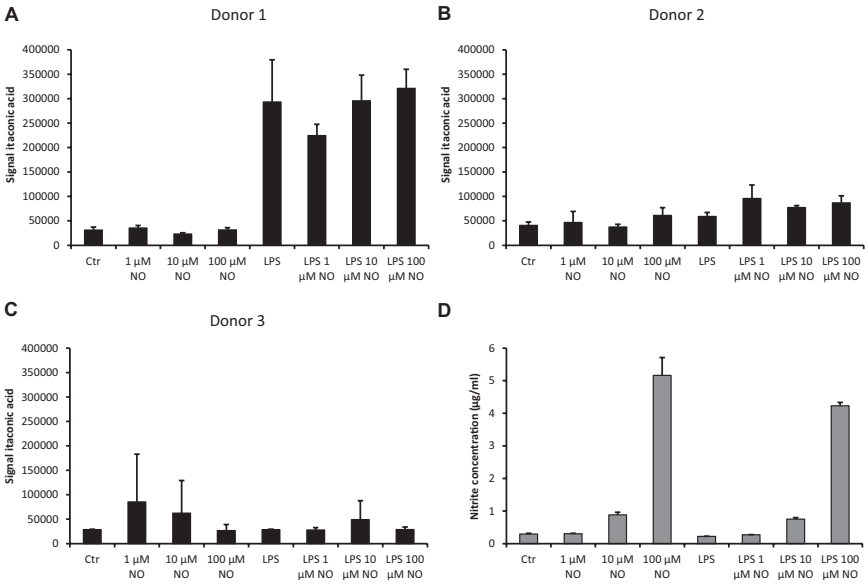

Fig. S6. (*A*–*C*) Itaconic acid levels in Ctr and LPS-activated (10 μg/mL) PBMC-derived macrophages from three donors treated with DEA NONOate at different concentrations (1, 10, 100 μM). Metabolites were harvested after 12 h of stimulation and the levels of itaconic acid were determined by GC/MS measurements. Each bar represents the mean of itaconic acid levels from three technical replicates (± SEM). (*D*) After 12 h, 180 μL of medium was harvested and combined with 20 μL 1 mM NaOH on ice to stop the dissociation reaction. Levels of nitrite were determined using the Griess assay and the concentrations were determined against a nitrite standard curve. Bars represent the mean of nitrite concentration (μg/mL) from the three donors (± SEM).

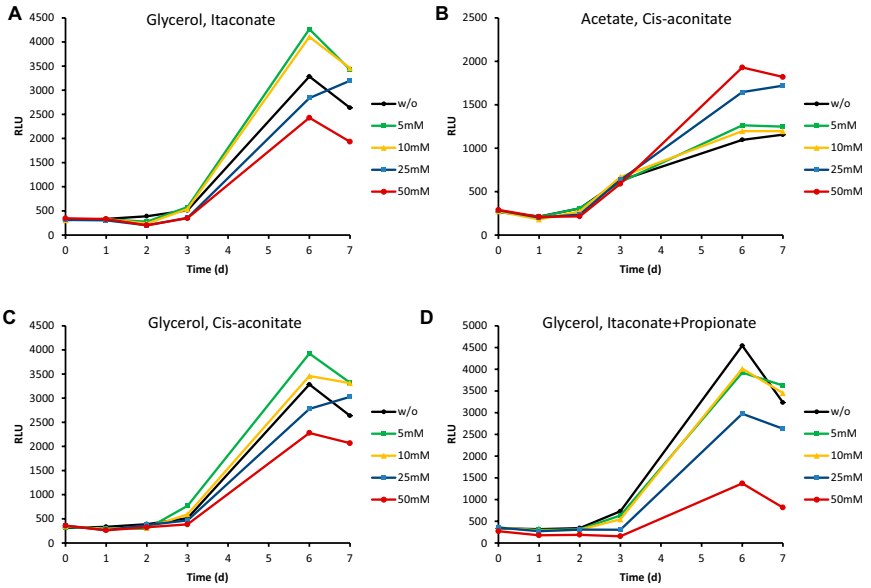

Fig. S7. GFP-expressing *Mycobacterium tuberculosis* bacteria were cultured in 7H9 medium supplemented with different carbon sources, without (w/o) and with various concentrations of itaconate (5, 10, 25, 50 mM) or *cis*-aconitate as indicated: (*A*) glycerol and itaconate, (*B*) acetate and *cis*-aconitate, (C) glycerol and *cis*-aconitate, and (*D*) glycerol, propionate, and itaconate. Growth was measured as relative light units (RLU) at indicated time points. Curves represent the mean of three technical replicates.

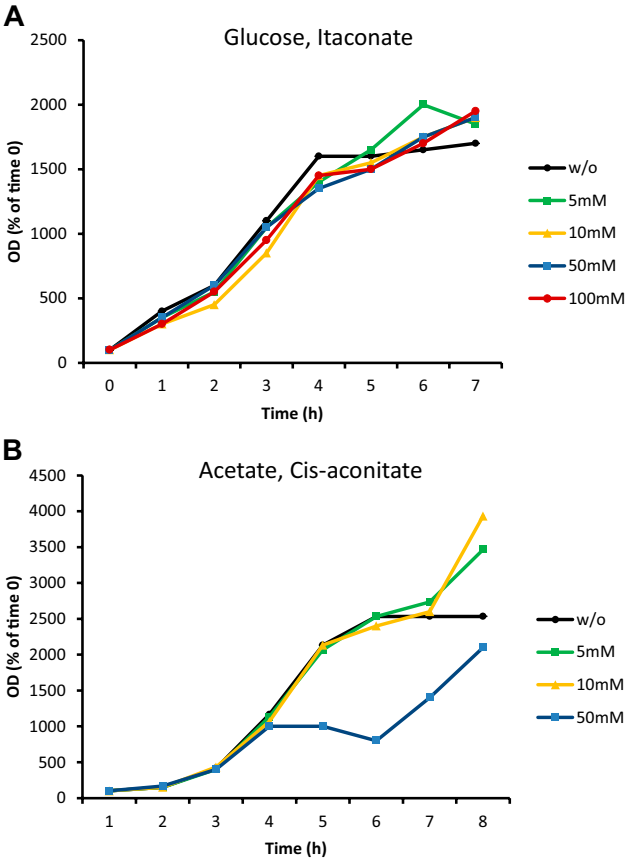

Fig. S8. (*A*) *Salmonella enterica* was grown in liquid medium with glucose in the presence of itaconic acid, and the OD was measured every hour (h). Curves represent the mean of two independent experiments. (*B*) *S. enterica* was grown in liquid medium with acetate as a unique carbon source without (w/o) or with increasing concentrations of *cis*-aconitate (5, 10, 50 mM). The OD was measured every hour to record the bacterial growth. Curves are calculated in the percent relative to time 0 and represent the mean of two independent experiments.

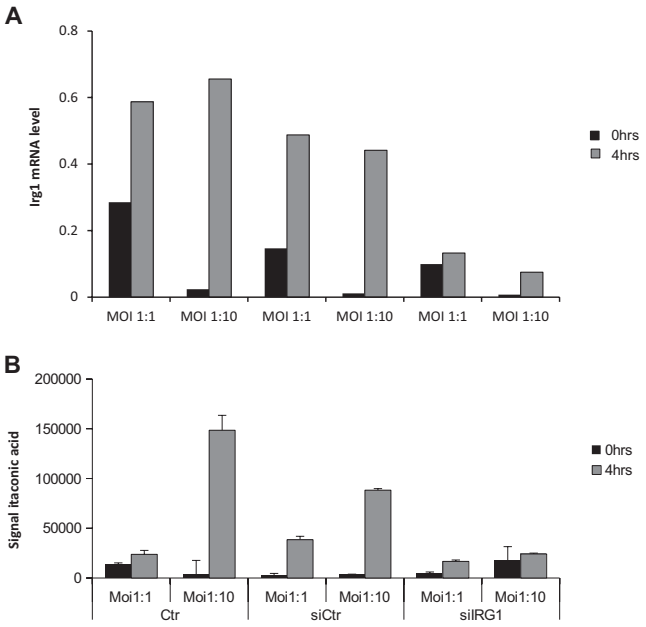

Fig. S9. (*A*) Levels of *Irg1* mRNA or (*B*) itaconic acid in RAW264.7 cells transfected with either siRNA specific for *Irg1* or with siRNA control under *S. enterica* infection at a multiplicity of infection (MOI) of 1:1 or 1:10 bacteria per macrophages. Infections were performed after 24 h of transfection and incubated for 0 h or 4 h after 1 h gentamycin exposure. Macrophages were then lysed to extract RNA and metabolites. Bars represent the results from one experiment.

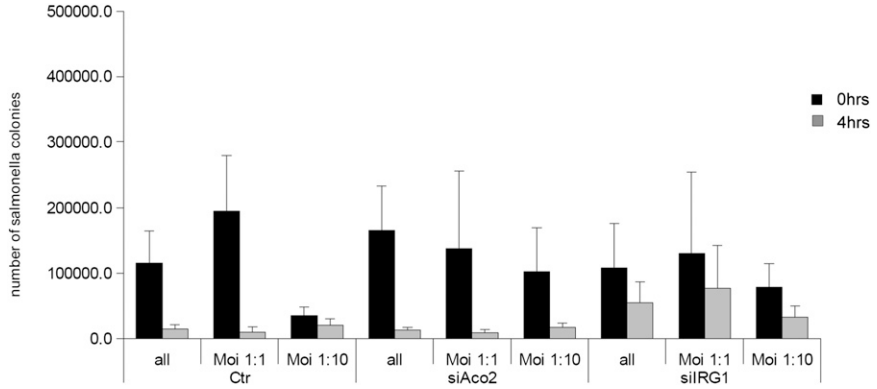

Fig. S10. Effect of *Irg1* silencing in macrophages on the bacterial growth. Mouse RAW264.7 cells were transfected with either siRNA specific for *Irg1* or with siRNA specific for murine aconitase 2 (*Aco2*) as control. Macrophages were infected with *S. enterica* at an MOI of 1:1 or 1:10 bacteria per macrophages. Infections were performed after 24 h of transfection and incubated for 0 h or 4 h after 1 h gentamycin exposure. Bars represent the mean of the numbers of colonies (± SEM) obtained from one experiment.